# Inkjet-Printed Humidity Sensor for Passive UHF RFID Systems

Juha Virtanen, *Student Member, IEEE*, Leena Ukkonen, *Member, IEEE*, Toni Björninen, *Member, IEEE*, Atef Z. Elsherbeni, *Fellow, IEEE*, and Lauri Sydänheimo, *Member, IEEE*

***Abstract*—This paper presents a novel inkjet-printed humidity sensor tag for passive radio-frequency identification (RFID) systems operating at ultrahigh frequencies (UHFs). During recent years, various humidity sensors have been developed by researchers around the world for HF and UHF RFID systems. However, to our best knowledge, the humidity sensor presented in this paper is one of the first passive UHF RFID humidity sensor tags fabricated using inkjet technology. This paper describes the structure and operation principle of the sensor tag as well as discusses the method of performing humidity measurements in practice. Furthermore, measurement results are presented, which include air humidity-sensitivity characterization and tag identification performance measurements.**

***Index Terms*—Inkjet, radio-frequency identification (RFIF), relative humidity (RH), sensor.**

## I. Introduction

RESEARCH involving radio-frequency identification (RFID) technology has seen a growing interest in sensing RFID tags as they could offer vast benefits over bar codes and traditional RFID tags. The main benefit would be improved product quality and safety throughout ubiquitous sensing. The research involving sensing RFID has resulted in various sensor tag designs such as accelerometers [1], displacement sensors [2], and temperature sensors [3].

One of the most popular sensor types for RFID systems is the humidity sensor, which is due to the great number of materials reacting to humidity-level variations. Humidity sensor tags have been developed for high-frequency (HF) RFID systems, [4] as well as for ultra-HF (UHF) RFID systems [5]–[8], and have been fabricated using either traditional photolithography or screen printing. The humidity sensor tag, which is presented in this paper, is fabricated using inkjet technology. Inkjet technology promises to bring cost-efficient and on-package RFID tags to markets [9]–[11]. In addition, it allows the use of polyimide film, which is the key component of the sensor, directly as the printing substrate.

This paper presents an improved novel inkjet-printed humidity sensor for passive UHF RFID systems. To our best knowledge, the developed sensor is one of the first passive UHF RFID humidity sensor tags fabricated using inkjet technology. The first humidity sensor tag design, along with numerical results, was presented in [12]. The humidity sensor tag, which is presented in this paper, has two major improvements as compared with the first version. First, the tag solely works in a passive operation mode, which has allowed further improvements for longer read range. Second, the sensor tag is based on a different and more sensitive RFID integrated circuit (IC).

The inkjet-printed humidity sensor tag finds applications not only as an air humidity sensor, i.e., hygrometer, but as a wireless structural humidity sensor able to indicate possible water damage early on. Moreover, this humidity sensor tag could be used to track environmental conditions during transportation of various goods, such as groceries and medicines.

In this paper, the operation of a passive RFID system, the structure of the sensor tag, and the operation principle of the humidity sensing are presented. Furthermore, a method to perform reliable humidity-level measurements using the sensor tag is proposed. The measurement results chapter includes numerical results acquired using Ansoft High-Frequency Structure Simulator (HFSS) and measurement data from air humidity-sensitivity characterization and tag identification performance measurements. The final chapter summarizes this paper and discusses future development involving the humidity sensor.

## II. Passive UHF RFID System

Passive UHF RFID systems mainly consist of three types of components, i.e., readers, tags, and end application, for example, database. The reader is essentially a transceiver operating at UHFs, and it is used to communicate with tags and with the end-user application. An RFID tag contains an antenna and an IC. The IC of the tag has an internal memory containing a unique electronic product code (EPC), which is used for identification purposes.

The operation of passive UHF RFID systems is based on coupling using electromagnetic (EM) waves. These EM waves are used by the reader and the tag to communicate with each other. Furthermore, the EM waves sent by the reader are used to provide operating power for passive RFID tags as they have no power supply of their own.

Manuscript received April 12, 2010; revised November 17, 2010; accepted February 1, 2011. Date of publication April 29, 2011; date of current version July 13, 2011. This work was supported in part by the Finnish Funding Agency for Technology and Innovation (TEKES), by the Academy of Finland, and by the Centennial Foundation of Finnish Technology Industries. The Associate Editor coordinating the review process for this paper was Dr. Deniz Gurkan.

J. Virtanen, L. Ukkonen, T. Björninen, and L. Sydänheimo are with Rauma Research Unit, Department of Electronics, Tampere University of Technology, 33720 Tampere, Finland.

A. Z. Elsherbeni is with the Department of Electrical Engineering, University of Mississippi, Oxford, MS 38677 USA.

Color versions of one or more of the figures in this paper are available online at http://ieeexplore.ieee.org.

Digital Object Identifier 10.1109/TIM.2011.2130070

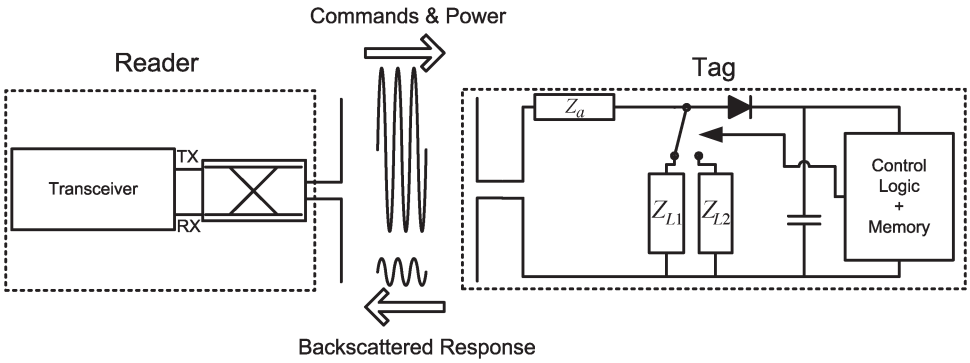


Fig. 1. Passive RFID system.

A passive RFID system is illustrated in Fig. 1. At the beginning of communication, the reader sends a continuous unmodulated carrier wave, which is received by the tag antenna. The incoming signal is routed to the IC, which uses its internal rectifier to transform the weak alternating current into direct current (dc). Next, internal voltage doublers are used to charge a capacitor, which acts as a power storage to allow short operation periods without the presence of the carrier wave. After the capacitor is charged to a sufficiently high dc voltage, the tag is activated and ready to receive commands from the reader [13].

The reader sends commands by means of amplitude shift keying (ASK), to which the tag replies by backscattering. In backscattering, the IC switches its input impedance between two states, i.e., reflecting and absorbing, according to the data contained in its internal memory, while the reader sends an unmodulated carrier wave. As the IC's input impedance is in the absorbing state, the input impedance is ideally the complex conjugate of the antenna impedance, allowing maximal power transfer between the antenna and IC. In the reflecting impedance state, the IC's input impedance is ideally short circuited, producing a complete power reflection of the carrier wave back to the reader [14]. By switching its input impedance, the IC produces either an ASK or phase shift keyed response, depending on the modulating impedance.

## III. Inkjet-Printed Humidity Sensor Tag

The developed humidity sensor tag is intended to be used for structural humidity monitoring, for example, inside floors and walls. The sensor tag can be used to quickly detect water damage, thus dramatically reducing the amount of additional damage caused by prolonged water exposure. The sensor tag is fully passive, and as such, it does not need any power supply of its own. Therefore, the sensor tag does not need any maintenance procedures, and it can be permanently enclosed inside walls, ceilings, and floors for long-term monitoring spanning several years. In addition, the sensor tag is flexible and small in size, allowing fitting inside various structures. This novel sensor tag has all the functionalities of an ordinary passive RFID tag, including the unique EPC code, which allows the use of several sensor tags in a small area as they can be recognized using their unique identification codes.

The sensor tag is still at a prototyping stage, and its development toward commercialization will require overcoming some challenges. First, inkjet fabrication processes are still few, limiting mass production volumes. Additionally, the durability and longevity of the printed ink is being researched to find out the environmental limits to the use of inkjet-printed electronics. However, considering the fast development in the area of inkjet printable electronics, it is reasonable to expect these challenges and unknowns to be solved in the near future.

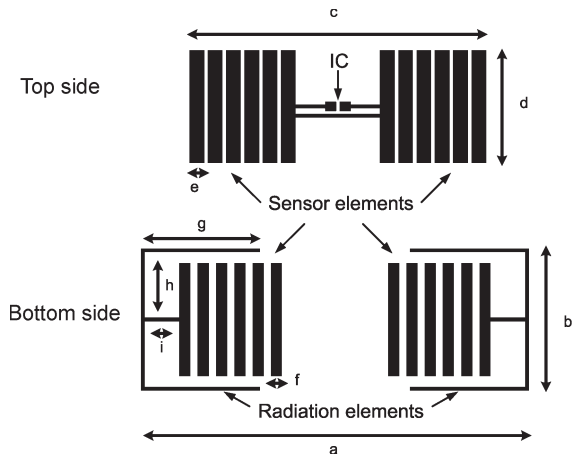


Fig. 2. Printing layout of the sensor tag.

### A. Structure of the Sensor Tag

The sensor tag is a double-sided structure formed by inkjet printing silver nanoparticle ink on 125-$\mu$m-thick Kapton 500 HN polyimide film by DuPont [15]. Harima NPS-J, a silver nanoparticle ink, was used to form the conductors of the tag. Harima NPS-J ink contains silver nanoparticles with a mean diameter of 12 nm and has a conductivity of 33 MS/m. The sensor tag consists of three main components: 1) an IC, which provides the basic identification functionality of the tag; 2) inkjet-printed sensor elements; and 3) radiation elements. The IC is a Higgs 3 RFID IC from Alien Technology [17]. The impedance of the IC and the radiating element are matched using a T-matching network to allow good power transfer between them and to maximize the read range of the sensor [18]. HFSS 12, which is a finite-element method EM simulator [19], was used to fine tune the dimensions of the impedance matching as well as the dimensions of the radiation elements to provide optimal performance. The printing layout of the sensor tag is shown in Fig. 2, and its key dimensions are shown in Table I.

TABLE I
KEY DIMENSIONS OF THE SENSOR TAG

| Dimension | a | b | c | d | e | f | g | h | i |
|---|---|---|---|---|---|---|---|---|---|
| Length [mm] | 106 | 39 | 81 | 31 | 4 | 3 | 31 | 18 | 10 |

The substrate, Kapton 500 HN, is a flexible, low loss, and extremely durable polyimide film dielectric. Kapton HN film was selected because of its special electrical properties: Kapton HN film's permittivity is dependent on the environmental humidity. This electrical property is the key factor in the sensor's functionality. Furthermore, Kapton HN is able to withstand the high-temperature levels, which the printed tag will undergo during sintering as a part of the inkjet printing process.

The sensor elements used in the sensor tag occupy both the top and bottom sides of the structure. These conductor plates form several parallel plate conductors, which are used to transform the variations in the permittivity of the substrate into electrical signal.

The radiation element is a short dipole antenna. Note that the sensor elements are also a part of the tag antenna. A dipole-type antenna was chosen due to its omnidirectional radiation pattern. This increases the reliability and usability of the sensor tag by minimizing the importance of the orientation of the tag or the reader antenna.

### B. Operation Principle

The humidity sensing of the tag is based on the humidity-dependent permittivity of the Kapton HN substrate. During a change in ambient humidity, the change in the substrate's permittivity is transformed into varying capacitance using the parallel plate capacitors. The varying capacitance, in turn, alters the impedance matching between the sensor elements and the IC, changing the tag's realized gain according to humidity.

Polyimide films, such as Kapton, are affected by changes in environmental humidity due to their internal chemical structure. Polyimide films are formed through heat-activated polycondensation. Moisture from the air absorbed by the polyimide causes a hydrolysis effect, which is the converse reaction of polycondensation. The hydrolysis effect causes the polyimide's internal carbon–nitrogen bonds to break, altering the internal electrical polarization. The altered electrical polarization effectively leads to altered permittivity of the polyimide [20].

Change in the Kapton HN film's permittivity due to environmental humidity is linear. According to the datasheet provided by DuPont, Kapton HN film's relative permittivity is 3.05 in an environmental relative humidity (RH) of 0% at 23 °C. The relative permittivity rises to a value of 3.85 when subjected to 100% RH at 23 °C. Thus, the humidity-dependent permittivity $\varepsilon_r(H)$ of the Kapton in 23 °C can be expressed as a function of ambient environmental humidity $H$ as follows:

$$\varepsilon_r(H) = 3.05 + 0.008 \times H. \quad (1)$$

Agilent 85070E Dielectric Probe Kit [21] was used to verify the permittivity of the Kapton HN film. The measurement ranged from 860 to 960 MHz. The measurement was repeated ten times, and the averaged result is shown in Fig. 3. The relative permittivity of the Kapton was found to be approximately 3.34 at the selected frequency band in indoor conditions. During the measurement, the environmental humidity was 32% RH at 23 °C, measured using a commercial hygrometer. The measured permittivity is in very good agreement with the relative permittivity given by the datasheet of Kapton HN. The measured permittivity shows some frequency dependence at the particular frequency band. However the variations in the measured permittivity are within ±0.01 and can be considered negligible.

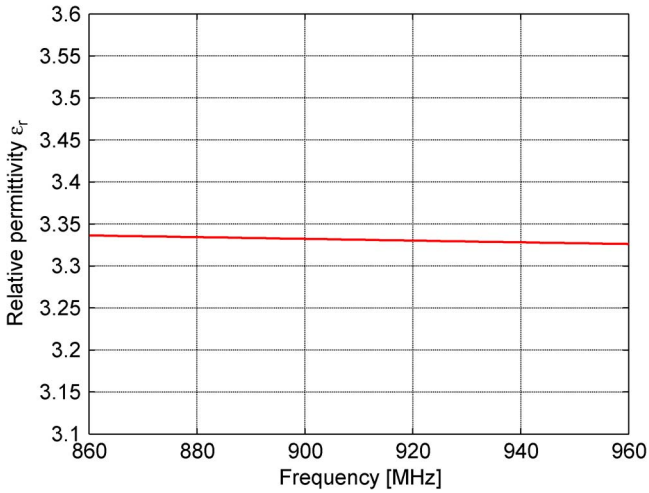


Fig. 3. Measured relative permittivity of a 1.5-mm-thick Kapton HN film from 860 to 960 MHz at 32% RH and at 23 °C.

The varying relative permittivity of the Kapton film is transformed into a capacitance, dependent on the environmental humidity using the parallel plate capacitors in the sensor elements. As the overall change in the capacitance is linearly related to the change in the relative permittivity of the dielectric, we are able to achieve a 28% overall change in the capacitance of the sensor elements between ambient humidity levels of 0% and 100% RH. Additional stray series capacitance, shown in Fig. 4, is also created by the adjacent plates. However, this capacitance can be considered to be negligible, as the parallel capacitance is the strongest; the parallel plate capacitors are separated by 125 $\mu$m, whereas the series capacitance is formed between plate edges separated by 1 mm apart.

The use of multiple parallel plate capacitors in the sensor elements is justified for two important reasons. First, by using several plate capacitors, an empty unprinted space between the capacitors is created. This empty space helps the polyimide to absorb moisture from the air. Second, the use of several capacitors maximizes the distance traveled by the signal current

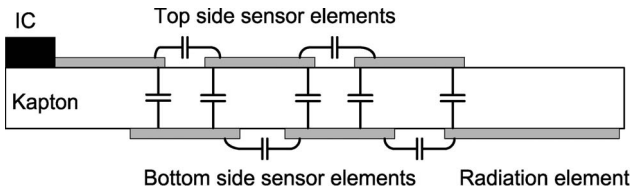


Fig. 4. Cross-sectional image of the sensor tag showing the capacitors, which are formed within the structure (not to scale and not including the entire sensor tag).

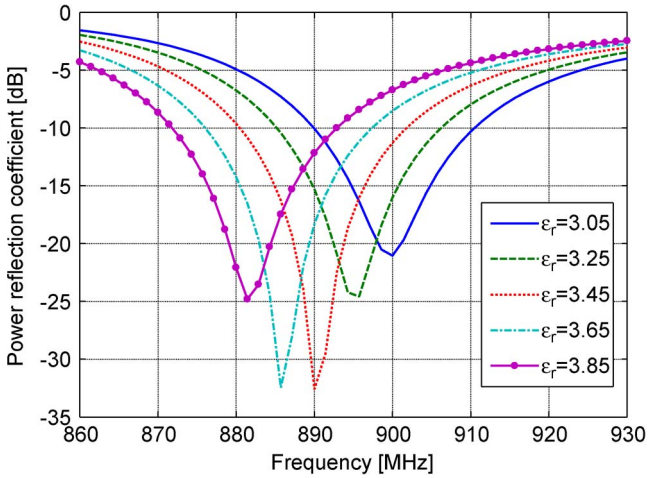


Fig. 5. Simulated power reflection coefficient.

inside the Kapton film, which should lead to a more humidity-sensitive operation.

Change in the capacitance, i.e., the input reactance of the sensor elements, affects the power transfer between the IC and the tag antenna throughout impedance matching. The magnitude of power transfer between a complex source (IC) and a complex load (sensor and radiation elements) can be best described by using the power reflection coefficient $\Gamma$ derived by Kurokawa in [22], i.e.,

$$\Gamma = \frac{P_R}{P_S} = \left| \frac{Z_L - Z_S^*}{Z_L + Z_S} \right|^2, \quad 0 \leq \Gamma \leq 1 \tag{2}$$

where $(Z_s^*)$ is the complex conjugate of the source impedance. The power reflection coefficient describes the ratio of the reflected power $P_R$ and the available power from the source $P_S$ for arbitrary complex source and load impedance values $Z_S$ and $Z_L$, respectively. The power reflection coefficient $\Gamma$ is analogous to $|S_{11}|^2$, as described in [23]. Low-magnitude power reflection is desirable since it provides the best overall power transfer and leads to maximal read range of the tag. Ideally, the load impedance should be the complex conjugate of the source impedance as it results in a zero power reflection coefficient. HFSS 12 was used to tune the impedance matching between the IC and the tag antenna.

Fig. 5 presents the simulated power reflection coefficient between the IC and the tag antenna with different substrate permittivities. In the simulation model, the input impedance of the RFID IC was modeled using values from [24], the conductors were modeled using a thickness of 3 $\mu$m and a conductivity of 33 MS/m. The losses in the dielectric layer were modeled using a loss tangent of 0.0025 at all frequencies.

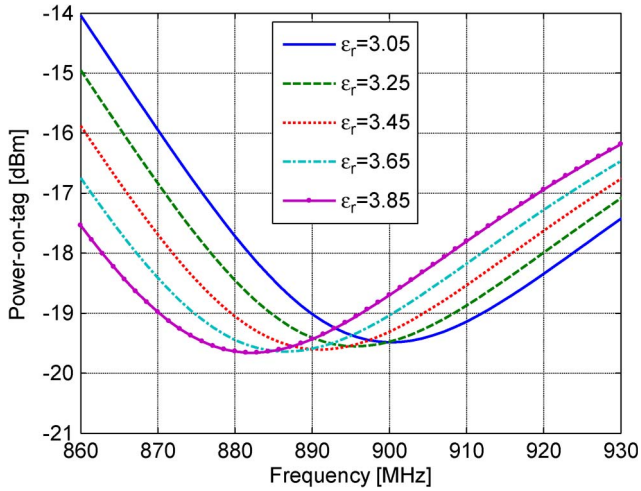


Fig. 6. Simulated power-on-tag using different substrate relative permittivities.

The humidity-dependent power reflection coefficient between the IC and the tag antenna cannot be directly measured using standard UHF RFID measurement equipment. Instead, in the actual measurements, the ambient humidity level is determined by measuring the power-on-tag $P_{\mathrm{on-tag}}$ of the tag as a function of frequency. The power-on-tag, assuming 0-dBi gain for the tag under test, is the minimum sufficient power available to the tag chip to activate it. Therefore, the power-on-tag can be considered as the sensitivity of the tag. The power-on-tag of the sensor is a function of ambient humidity as it is affected by the power transfer between the tag antenna and the IC. The humidity-dependent power-on-tag $P_{\mathrm{on-tag}}(H)$ of the sensor is given by

$$P_{\mathrm{on-tag}}(H) = L_{\mathrm{fwd}} P_{\mathrm{TS}} = \frac{P_{\mathrm{IC}}}{G_{\mathrm{tag}} \times (1 - \Gamma)} \tag{3}$$

where $L_{\mathrm{fwd}}$ is the path loss in the forward link, i.e., from the reader to the tag, including the cable and polarization losses and the gain of the reader antenna, between the tag and the reader. $P_{\mathrm{TS}}$ is the transmit power at the antenna port needed to activate the tag, i.e., threshold power, $P_{\mathrm{IC}}$ is the sensitivity of the RFID IC, and $G_{\mathrm{tag}}$ is the gain of the tag antenna. The use of power-on-tag as the measurand provides enhanced robustness against fading environments: The reflections of the environment are counteracted by the measured path loss.

Fig. 6 presents a simulated power-on-tag of the sensor tag as the substrate's relative permittivity changes due to humidity. The sensitivity of the IC was assumed to be a constant $-18$ dBm. The power-on-tag of the sensor mainly experiences a frequency shift at different ambient air humidity levels.

### C. Ambient Humidity-Level Measurement

In practice, the measurement of humidity is done by using two tags: one acts as the sensor, and the other as a stable reference. This type of measurement setup has been successfully used by other researchers working with RFID humidity

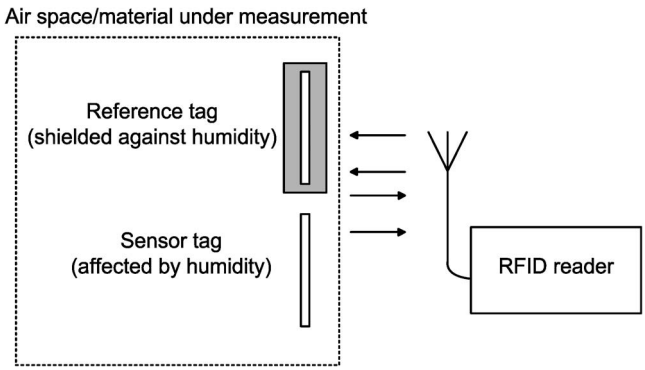


Fig. 7. Measurement setup while measuring ambient humidity.

sensors [25]. The reference tag is carefully designed to exhibit a certain frequency response, and only this tag is intended for this purpose. Furthermore, the reference and the sensor tags are used as a whole, i.e., the reference tag is always at a fixed orientation and distance to the actual sensor tag.

The sensor tag is placed at the selected location under measurement that is exposed to the ambient humidity. The reference tag is shielded in a casing of dielectric impervious to humidity. As a result, the power-on-tag of the reference tag is unaffected by the humidity, whereas the power-on-tag of the sensor tag changes according to the ambient humidity level. This measurement setup is illustrated in Fig. 7.

At the beginning of a humidity measurement, a calibration is performed using the reference. In the calibration, the measurement system measures the forward link path loss $L_{\mathrm{fwd}}$ between the reference and the reader antenna. This path loss measurement is possible by knowing the exact operation characteristics, i.e., power-on-tag response of the reference tag. After the calibration, a power-on-tag measurement is performed on both tags as a function of frequency. The ambient humidity level is extracted from the frequency difference in the measured frequency points of lowest power-on-tag values of the sensor and the reference.

The key point in this method is to form a relation between the amount of frequency difference in the power-on-tag curves of the reference and the sensor and the ambient humidity value. This can be done via simulations or calibration measurements.

Humidity sensitivity $S$ can be used to indicate how much frequency difference is generated between the reference tag's and sensor tag's frequency points of lowest power-on-tag by one percent change in the RH level. This sensitivity to humidity can be defined as

$$S = \frac{|\Delta f|}{|\Delta H|} = \frac{f_{\mathrm{Humid}} - f_{\mathrm{Dry}}}{|H_{\mathrm{Humid}} - H_{\mathrm{Dry}}|} \tag{4}$$

where $|\Delta H|$ is the total change in the humidity level between humidity levels $H_{\mathrm{Dry}}$ and $H_{\mathrm{Humid}}$. $H_{\mathrm{Dry}}$ corresponds to a low humidity level, ideally 0% RH, whereas the $H_{\mathrm{Humid}}$ corresponds to a high humidity level, ideally 100% RH. The term $|\Delta f|$ stands for the total frequency difference in the frequency points of lowest power-on-tag. $f_{\mathrm{Dry}}$ is the frequency point of the lowest power-on-tag level at humidity level $H_{\mathrm{Dry}}$. Whereas, $f_{\mathrm{Humid}}$ is the frequency point of the lowest power-on-tag level at the humidity level of $H_{\mathrm{Humid}}$.

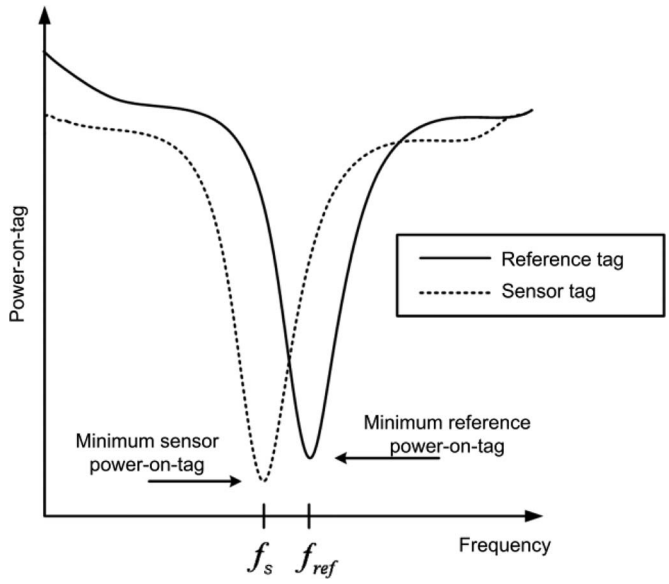


Fig. 8. Illustration of the power-on-tag curves measured during a humidity-level measurement.

After determining the humidity sensitivity $S$ of the sensor tag through measurements or simulations, one is able to conduct the actual humidity measurement throughout power-on-tag sweeps. Fig. 8 illustrates the resulting power-on-tag curves during a humidity measurement.

Using the humidity sensitivity $S$, the environmental humidity can be acquired using the following expression:

$$H_M = |\Delta f_M| \times S^{-1} = |f_{\mathrm{ref}} - f_m| \times S^{-1} \tag{5}$$

where $H_M$ is the measured ambient humidity level in percentage RH, $S$ is the humidity sensitivity of the sensor tag, and $|\Delta f_M|$ is the measured frequency difference between the reference tag's and sensor's frequency points of lowest threshold power. Equation (5) assumes that the reference tag is designed to have its frequency point of lowest power-on-tag at the same frequency as the sensor tag's frequency point of lowest power-on-tag at an RH level of 0%.

## IV. Manufactured Samples

Sensor tag samples were manufactured in the Laboratory of Printable Electronics, Department of Electronics, Tampere University of Technology. Printing was made using an iTi XY MDS 2.0 inkjet printer, equipped with Spectra S class print heads. The printing resolution was set to 600 dpi. Using these parameters, the inkjet printing process should produce a conductor thickness ranging from 1.0 to 1.5 $\mu$m per printing layer. Samples were printed using two ink layers to reduce the losses caused by the skin effect. The IC strap was attached by hands using conductive epoxy resin. Adhesive tape was laid on top of the IC to protect it from excessive humidity levels. Fig. 9 shows a single printed humidity sensor tag from both sides.

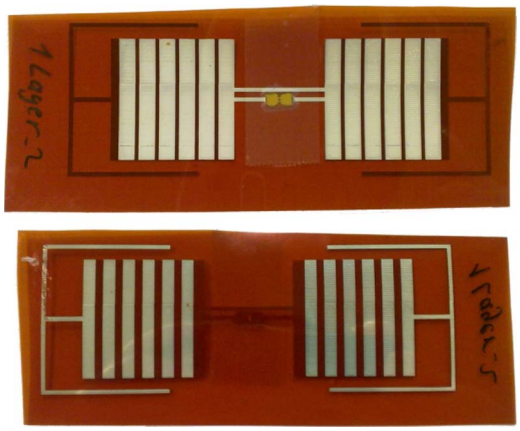

Fig. 9. Inkjet-printed sensor tag.

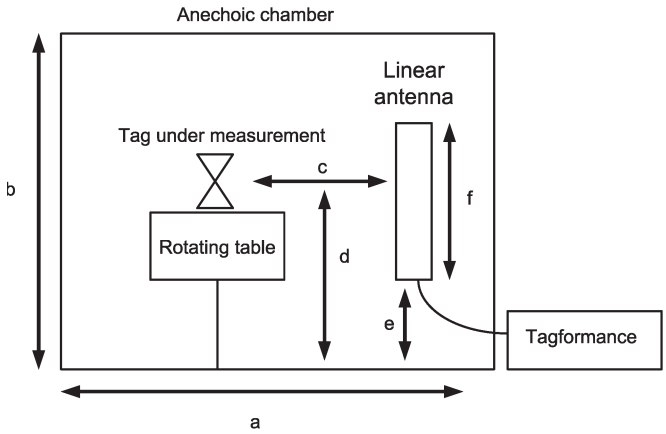


Fig. 10. Side view of the measurement setup.

## V. Measurement Results

The measurements in this paper were conducted in an anechoic RFID measurement chamber using a setup shown in Fig. 10. The key dimensions of the measurement setup are listed in Table II. The anechoic chamber, with a built-in rotating table, is designed particularly for UHF RFID tag performance measurements. A monostatic reader antenna configuration, i.e., a single linear reader antenna, SPA 800/76/8/0 V from Huber–Suhner, was used to transmit and to receiver power.

Tagformance measurement system [26] was used to perform power-on-tag and radiation pattern measurements carried out for this paper. The core operations of this system are performed with a vector signal analyzer. The Tagformance measurement system's capability to perform power-on-tag measurements is enabled by a calibration step, performed at the beginning of measurements.

The calibration data, i.e., the forward link path loss $L_{\mathrm{fwd}}$, is shown in Fig. 11. The calibration data has four discontinuities; these are caused by the measurement resolution of the Tagformance system during calibration. The frequency step during calibration is fixed to 1 MHz and the power step to 0.1 dB. However, these discontinuities in the measured forward path loss are small and do not have any significant affect on the measurement results.

### A. Characterization of Humidity Sensitivity

This section presents the measurement results of the humidity-sensitivity characterization performed at a constant ambient air temperature of 24 °C. In these measurements, the sensor tag was placed inside a 5-L plastic jar along with different salt solutions to create stable humidity conditions. The salt solutions, commonly used to calibrate commercial humidity meters, were acquired from Vaisala Ltd. The salt solutions used and their equilibrium RH levels are shown in Table III [27, Table 2, p. 92].

The measurement procedure for each salt solution was as follows.

1) Calibration was performed using the reference tag of the Tagformance system.
2) The salt solution was formed and poured into the bottom of the jar.
3) The sensor tag was hung by plastic wires in the middle of the jar volume.
4) The jar, containing the salt solution and the sensor, was sealed and placed to the anechoic chamber and left to sit for 12 h.
5) After the humidity value was settled (humidity values were verified using a commercial hygrometer), five consecutive threshold power sweeps were performed from 800 MHz to 1 GHz using 0.2-MHz frequency and 0.1-dB power steps.
6) The power-on-tag results were calculated from the threshold power sweeps using (3) with the calibration data shown in Fig. 11.
7) The measured power-on-tag curves were postprocessed using Mathworks MATLAB to obtain the frequency point of the lowest power-on-tag from and the standard deviation for all of the frequency points of lowest power-on-tag results.

Figs. 12–15 display the measured power-on-tag levels at 11%, 33%, 75%, and 97% RH. Additionally, these figures contain envelopes drawn using minimal and maximal measured power-on-tag values.

The measured and simulated power-on-tag results have similar center frequencies. However, the simulated and measured levels of power-on-tag significantly differ. The difference in the levels of the power-on-tag is most likely caused by the fact that the exact conductivity and layer thickness of the silver ink are not known and clearly differ from the values used in the simulations. The slight frequency offset between the simulated and measured power-on-tags is caused by the fact that the IC was attached by hand. The manual attachment has introduced some parasitic elements, e.g., stray capacitances, which were not included in the simulation model.

*1) Postprocessed Results:* The sensor tag's measured power-on-tag does not exhibit any single unambiguous frequency point of lowest power-on-tag. Instead, the measured power-on-tag usually stays nearly constant in the vicinity of the center frequency of the lowest power-on-tag. This is due to the power step resolution, with 0.1 dB being the lowest step: the change in the tag's power-on-tag level close to the actual point of best operation, i.e., at the lowest power-on-tag level, is less than 0.1 dB.

TABLE II
KEY DIMENSIONS OF THE MEASUREMENT SETUP

| Dimension | a | b | c | d | e | f |
|---|---|---|---|---|---|---|
| Distance [cm] | 120 | 80 | 45 | 39 | 28 | 25 |

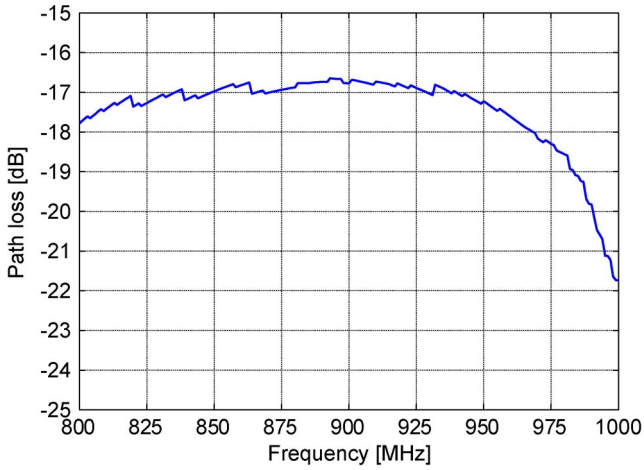


Fig. 11. Calibration data used in the measurements made for this paper.

TABLE III
SALT SOLUTIONS AND THEIR EQUILIBRIUM RELATIVE HUMIDITY LEVELS AT 24 °C

| Salt solution | Equilibrium relative humidity [%] |
|---|---|
| Lithium Chloride, LiCl | 11.3 ± 0.3 |
| Magnesium Chloride, $MgCl_2$ | 32.8 ± 0.2 |
| Sodium Chloride, NaCl | 75.1 ± 0.1 |
| Potassium Sulfate, $K_2SO_4$ | 97.3 ± 0.5 |

To counteract this, MATLAB is used to find the unambiguous frequency point of the lowest measured power-on-tag $f_{\min-P_{\rm on}}$ from Figs. 12–15. First, a search is made for all frequency points, which satisfy the following condition:

$$P_{\rm on}(f) - \min(P_{\rm on}) < y, \quad 0.1 \le y \le 0.5 \tag{6}$$

where $P_{\rm on}(f)$ is the measured power-on-tag as a function of frequency, $\min(P_{\rm on})$ is the magnitude of the lowest measured power-on-tag, and $y$ is a constant. The purpose of $y$ is to diminish any effects of possible random measurement errors from the power-on-tag level. The MATLAB code used selects the $y$ value from the prespecified range, which produces the smallest standard deviation in the resulting frequency points. The unambiguous frequency point of the lowest power-on-tag $f_{\min-P_{\rm on}}$ is found from the mean of these frequency points, satisfying (6). This method is valid as if it is assumed that the unambiguous frequency point of lowest power-on-tag is found from the center point of the valley in the measured power-on-tag. This assumption is true based on the simulated power-on-tag.

Table IV presents the mean values, acquired using the method described, for the frequency points of the lowest power-on-tag in various humidity levels and the standard deviations in the obtained frequency points.

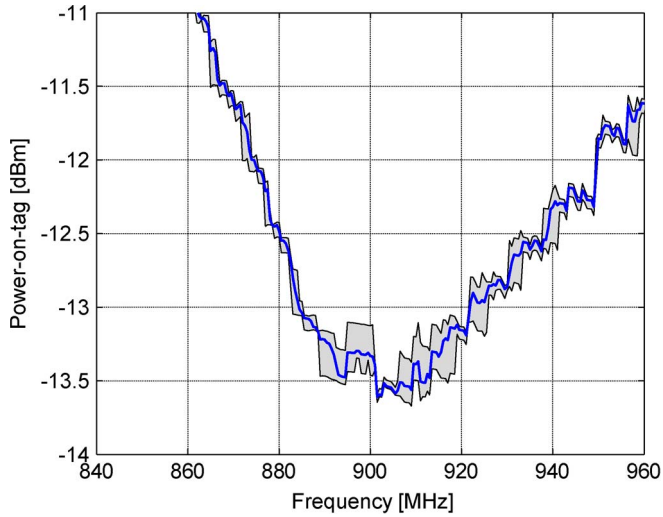


Fig. 12. Measured power-on-tag at 11% RH ambient air humidity.

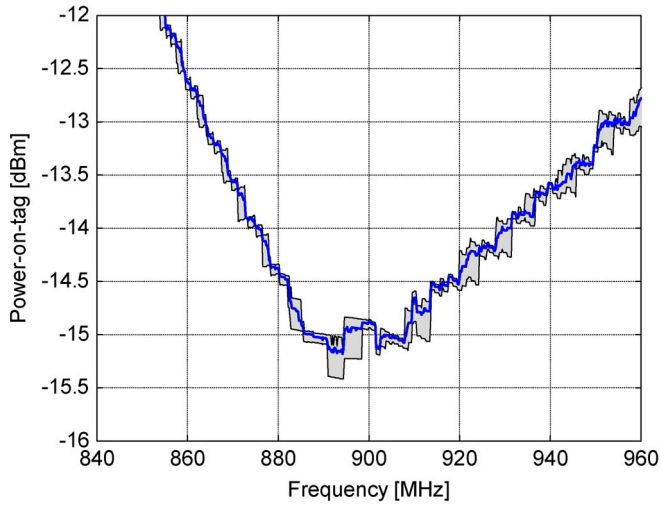


Fig. 13. Measured power-on-tag at 33% RH ambient air humidity.

Using the measurement data from Table IV, weighted least-squares (WLS) fitting was used to obtain the humidity sensitivity $S$ of the sensor. Weighting was done using the inverse variance related to each measurement. The humidity sensitivity of the sensor can be found from the absolute value of the slope of the linear regression. The polynomial for the frequency point of the lowest power-on-tag $f_{\min-P_{\rm on}}$ in MHz becomes

$$f_{\min-P_{\rm on}} = (-0.1988 \times H + 904.2757)\ \text{MHz} \tag{7}$$

where $H$ is the relative air humidity in percentage. The standard deviations in the slope and intercept are 0.0149 and 0.5291,

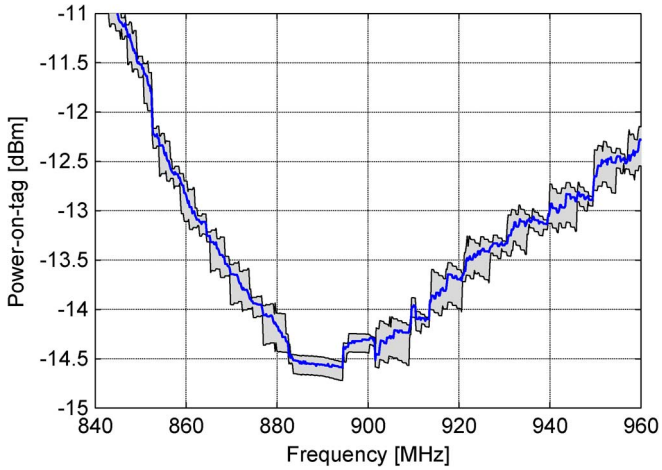


Fig. 14. Measured power-on-tag at 75% RH ambient air humidity.

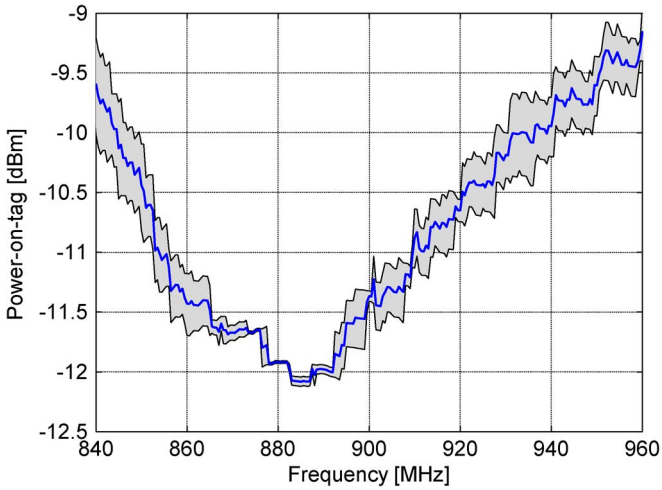


Fig. 15. Measured power-on-tag at 97% RH ambient air humidity.

respectively. The measured humidity sensitivity $S$ is the absolute value of the slope of $f_{\min - P_{\rm on}}$, i.e.,

$$S = \frac{|\Delta f|}{|\Delta H|} = \frac{(198.8 \pm 14.9)\text{kHz}}{\%\text{RH}}. \tag{8}$$

A sensitivity $S$ of 171.4 kHz/%RH is obtained by applying the same postprocessing method to the simulated power-on-tag data, as shown in Fig. 6. The difference between the measured and simulated humidity sensitivity is most likely caused by the water absorption differences: In the simulation model, the humidity is being uniformly absorbed; in reality, the humidity absorption is affected by the conductors, causing an uneven water distribution within the Kapton film. Fig. 16 presents the measured frequency points of the lowest power-on-tag and the WLS solution of the measured sensitivity.

The measured humidity sensitivity in (8) allows humidity measurements within $\pm 4.0\%$ RH accuracy. This uncertainty could be minimized by performing additional power-on-tag measurements during the humidity-sensitivity characterization, thus lowering the standard deviation in the linear regression.

### B. Identification Performance

The theoretical read range $d_{\rm tag}$, which determines the maximal distance at which one is able to conduct humidity measurements using the sensor tag in free space, is given by [28]

$$d_{\rm tag} = \frac{\lambda}{4\pi}\sqrt{\frac{P_{\rm EIRP}}{L_{\rm fwd} P_{\rm TS}}} \tag{9}$$

where $P_{\rm EIRP}$ stands for the maximum equivalent isotropically radiated power (EIRP) allowed by local European regulations (3.28 W) [29]. The parameter $L_{\rm fwd}$ is the measured path loss in the forward link. The term $P_{\rm TS}$ stands for the corresponding threshold power level measured as a function of transmit frequency. The results for the averaged theoretical read ranges of the sensor tag in different humidity levels at 24 °C are shown in Fig. 17.

The sensor tag, printed with two ink layers, can be operated from a maximum distance of 8.7 m in free space. In practice, the read range of the sensor tag will be lower as any obstacles, such as walls, will cause attenuation. However, the read range could be increased by printing additional ink layers to increase the conductor thickness [30].

The measured radiation pattern of the sensor tag, as shown in Fig. 18, shows the normalized patterns in the $\varphi$ and $\theta$ planes. The measurement was performed at 885 MHz, at 33% RH, and at 24 °C. The $\theta$-plane of the tag is measured by rotating the dipole tag along its electric field vector. The $\varphi$-plane is measured by rotating the dipole tag along its magnetic field vector. Measurements showed a slight difference in the front and back lobes in the $\theta$ and $\varphi$ planes. However, this difference was not visible in our numerical radiation patterns, and it is probably caused by fabrication tolerances, e.g., aligning of the top and bottom layers.

## VI. Conclusion and Future Work

This paper has presented an improved version of the novel humidity sensor tag for UHF RFID systems, which was originally presented in [12]. Extensive measurements that were performed acquire the humidity sensitivity of the sensor. The humidity sensitivity of the sensor was found to be 198.8 ± 14 kHz/%RH. The measured standard deviation in the humidity sensitivity allows humidity measurements within ±4.0% RH accuracy. Even greater accuracy could be obtained by using a smaller frequency step in the measurements. However, this will increase the overall time required by the measurement. The identification performance of the sensor tag has been found to be comparable to a traditional RFID tag; the read range of the sensor, i.e., the operating range, was approximately 8 m at various humidity levels.

In the future, a special narrow bandwidth reference tag will be designed to allow humidity level measurements using the measurement method described in this paper. These humidity level measurements will be performed in practical applications and in fading environments. The resulting measurement data will be used to assess the accuracy, reliability, and usability of the humidity measurement method. The additional operation characteristics of the sensor tag, for example, its hysteresis

TABLE IV
MEAN FREQUENCY POINTS OF THE LOWEST POWER-ON-TAG AND THEIR STANDARD DEVIATIONS

| Relative air humidity at 24 °C [%] | Mean frequency point of lowest power-on-tag [MHz] | Standard deviation σ [MHz] |
|---|---|---|
| 11.3 | 903.3985 | 0.5345 |
| 32.8 | 897.6628 | 0.0681 |
| 75.1 | 889.7235 | 0.5035 |
| 97.3 | 885.2500 | 0.6142 |

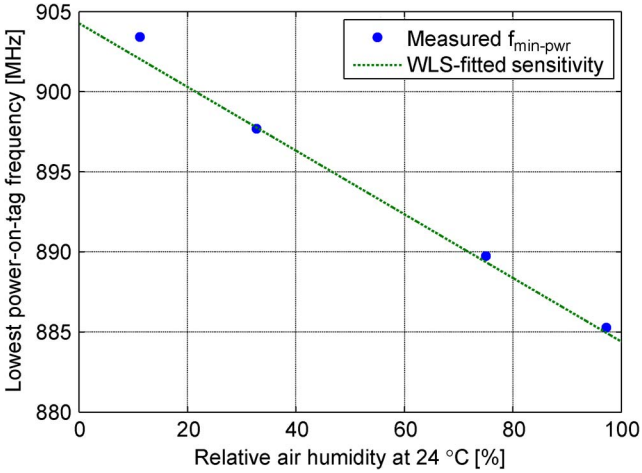


Fig. 16. Measured frequency points of the lowest power-on-tag as a function of relative air humidity.

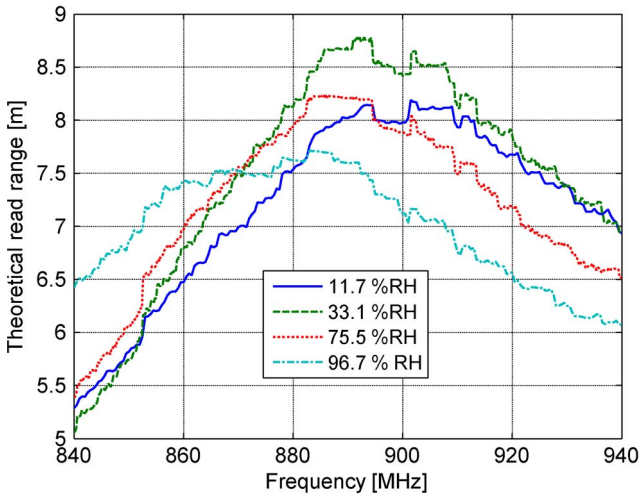


Fig. 17. Measured theoretical read range of the sensor at different ambient humidity levels at24 °C.

and response time, will be also studied in future research. Furthermore, custom RFID reader software will be developed, which will perform automatic humidity-level measurements using the method proposed in this paper.

## ACKNOWLEDGMENT

The authors would like to thank Dr. T. Joutsenoja and Dr. K. Kaija for their help in manufacturing the printed sensor tags. The authors would also like to thank A. A. Babar for performing the permittivity measurements.

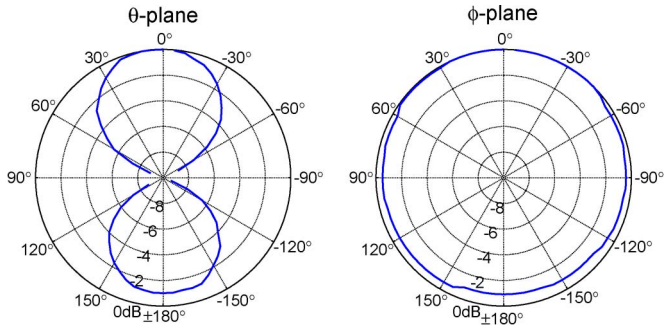


Fig. 18. Normalized free-space radiation patterns in $\varphi$ and $\theta$ planes measured at 885 MHz.

## REFERENCES

[1] M. Philipose, J. R. Smith, B. Jiang, A. Mamishev, R. Sumit, and K. Sundara-Rajan, "Battery-free wireless identification and sensing," *IEEE Pervasive Comput. Mag.*, vol. 4, no. 1, pp. 37–45, Jan.–Mar. 2005.

[2] R. Bhattacharyya, C. Floerkemeier, and S. Sarma, "Towards tag antenna based sensing—An RFID displacement sensor," in *Proc. IEEE Int. Conf. RFID*, Orlando, FL, 2009, pp. 95–102.

[3] K. Opasjumruskit, T. Thanthipwan, O. Sathusen, P. Sirinamarattana, P. Gadmanee, E. Pootarapan, N. Wongkomet, A. Thanachayanont, and M. Thamsirianunt, "Self-powered wireless temperature sensors exploit RFID technology," *IEEE Pervasive Comput. Mag.*, vol. 5, no. 1, pp. 54–61, Jan.–Mar. 2006.

[4] J. Voutilainen, "Methods and instrumentation for measuring moisture in building structures," Ph.D. dissertation, Helsinki Univ. Technol., Espoo, Finland, 2005.

[5] K. Chang, Y. H. Kim, Y. J. Kim, and Y. J. Yoon, "Functional antenna integrated with relative humidity sensor using synthesised polyimide for passive RFID sensing," *Electron. Lett.*, vol. 43, no. 5, pp. 7–8, Mar. 2007.

[6] J. Yi, M. Heiss, F. Qiuyun, and N. A. Gay, "A prototype RFID humidity sensor for built environment monitoring," in *Proc. Educ. Technol. Training & Int. Workshop Geosci. Remote Sens.*, Shanghai, China, 2008, pp. 496–499.

[7] A. Oprea, N. Barsan, U. Weimar, M. Bauersfeld, D. Ebling, and J. Wollenstein, "Capacitive humidity sensors on flexible RFID labels," *Sens. Actuators B, Chem.*, vol. 132, no. 2, pp. 404–410, Jun. 2008.

[8] A. Oprea, N. Barsan, U. Weimar, M. Bauersfeld, D. Ebling, and J. Wollenstein, "Capacitive humidity sensors on flexible RFID labels," in *Transducers/Eurosensors XXI, Proc. The 14th Int. Conf. Solid-State Sens., Actuators Microsyst. and 21st Eur. Conf. Solid-State Transducers*, 2007, pp. 2039–2042.

[9] Z. Konstas, A. Rida, R. Vyas, K. Katsibas, N. Uzunoglu, and M. M. Tentzeris, "A novel 'Green' inkjet-printed Z-shaped monopole antenna for RFID applications," in *Proc. 3rd European Conf. Antennas Propag.*, Berlin, Germany, 2009, pp. 2340–2343.

[10] Y. Amin, S. Prokkola, S. Botao, J. Hallstedt, H. Tenhunen, and Z. Li-Rong, "Inkjet printed paper based quadrate bowtie antennas for UHF RFID tags," in *Proc. 11th Int. Conf. Adv. Commun. Technol.*, Phoenix Park, Korea, 2009, vol. 1, pp. 109–112.

[11] L. Hakola, Benefits of Inkjet Printing for Printed Electronics, 2005. VTT, Pira Printed Electronics, viewed on Nov. 11, 2010. [Online]. Available: http://www3.vtt.fi/liitetiedostot/cluster5_metsa_kemia_ymparisto/PIRA%20Printed%20Electronics%202005%20Hakola.pdf
[12] J. Virtanen, L. Ukkonen, T. Bjorninen, and L. Sydanheimo, "Printed humidity sensor for UHF RFID systems," in *Proc. IEEE SAS*, Limerick, Ireland, Feb. 23–25, 2010, pp. 269–272.
[13] D. M. Dobkin, *The RF in RFID: Passive UHF RFID in Practice*. Amsterdam, The Netherlands: Elsevier, 2008.
[14] J. P. Curty, N. Joehl, C. Dehollain, and M. J. Declercq, "Remotely powered addressable UHF RFID integrated system," *IEEE J. Solid-State Circuits*, vol. 40, no. 11, pp. 2193–2202, Nov. 2005.
[15] Kapton HN Polyimide Film, Datasheet, Sep. 9, 2010. [Online]. Available: http://www2.dupont.com/Kapton/en_US/index.html
[16] Harima NPS-J NanoPaste: Metal Paste for Fine Pattern Formation, Datasheet, Sep. 9, 2010. [Online]. Available: http://www.harima.co.jp/en/products/pdf/16-17e.pdf
[17] Alien Technology, Alien Higgs 3 Product Overview, Sep. 9, 2010. [Online]. Available: http://www.alientechnology.com/docs/products/DS_H3.pdf
[18] G. Marrocco, "The art of UHF RFID antenna design: Impedance-matching and size-reduction techniques," *IEEE Antennas Propag. Mag.*, vol. 50, no. 1, pp. 66–79, Feb. 2008.
[19] Ansoft High Frequency Structure Simulator, HFSS 12, Overview, Sep. 9, 2010. [Online]. Available: http://www.ansoft.com/products/hf/hfss/
[20] A. R. K. Ralston, C. F. Klein, P. E. Thomas, and D. D. Denton, "A model for the relative environmental stability of a series of polyimide capacitance humidity sensors," in *Proc. 8th Int. Conf. Solid-State Sens. Actuators, and Eurosensors IX, Transducers*, 1995, vol. 2, pp. 821–824.
[21] Agilent 85070E Dielectric Probe Kit Technical Overview, Sep. 9, 2010. [Online]. Available: http://cp.literature.agilent.com/litweb/pdf/5989-0222EN.pdf
[22] K. Kurokawa, "Power waves and the scattering matrix," *IEEE Trans. Microw. Theory Tech.*, vol. MTT-13, no. 2, pp. 194–202, Mar. 1965.
[23] P. V. Nikitin, K. V. S. Rao, S. F. Lam, V. Pillai, R. Martinez, and H. Heinrich, "Power reflection coefficient analysis for complex impedances in RFID tag design," *IEEE Trans. Microw. Theory Tech.*, vol. 53, no. 9, pp. 2721–2725, Sep. 2005.
[24] T. Björninen, M. Lauri, L. Ukkonen, L. Sydänheimo, A. Elsherbeni, and R. Ritala, "Wireless measurement of UHF RFID chip impedance," in *Proc. 32nd AMTA Symp.*, Atlanta, GA, 2010, pp. 35–40.
[25] J. Sidén, Z. Xuezhi, T. Unander, A. Koptyug, and H. E. Nilsson, "Remote moisture sensing utilizing ordinary RFID tags," in *Proc. IEEE Sensors*, Oct. 2007, pp. 308–311.
[26] Tagformance, Product Brochure, Sep. 9, 2010. [Online]. Available: http://www.voyantic.com/
[27] L. Greenspan, "Humidity fixed points of binary saturated aqueous solutions," *J. Res. Nat. Bureau Std.—A. Phys. Chem.*, vol. 81A, no. 1, pp. 89–95, Jan./Feb. 1977.
[28] P. V. Nikitin and K. V. S. Rao, "Antennas and propagation in UHF RFID systems," in *Proc. IEEE Int. Conf. RFID*, Las Vegas, NV, 2008, pp. 277–288.
[29] EPC Global, Frequency Regulations, Sep. 9, 2010. [Online]. Available: http://www.epcglobalinc.org/tech/freq_reg/RFID_at_UHF_Regulations_20100824.pdf
[30] J. Virtanen, T. Björninen, L. Ukkonen, K. Kaija, T. Joutsenoja, L. Sydänheimo, and A. Z. Elsherbeni, "The effect of conductor thickness in passive inkjet printed RFID tags," in *Proc. IEEE Int. Symp. Antennas Propag. & CNC/USNC/URSI Radio Sci. Meeting*, Toronto, ON, Canada, Jul. 11–17, 2010, pp. 1–4.

**Juha Virtanen** (S'09) received the M.Sc. degree in electrical engineering in 2009 from Tampere University of Technology (TUT), Tampere, Finland, where he is currently working toward the Ph.D. degree in electrical engineering.

He is currently working as a Researcher with the Department of Electronics, Rauma Research Unit, TUT. He has authored publications on ultrahigh-frequency radio-frequency identification (UHF RFID) sensor tags and printable electronics for microwave applications. His research interests include sensor integration into UHF RFID systems and the development of passive inkjet-printed UHF RFID tags.

**Leena Ukkonen** (M'03) received the M.Sc. and Ph.D. degrees in electrical engineering from Tampere University of Technology (TUT), Tampere, Finland, in 2003 and 2006, respectively.

She is currently leading the RFID Research Group, Department of Electronics, Rauma Research Unit, TUT. She is the holder of the Adjunct Professorship at Aalto University School of Science and Technology, Espoo, Finland. She has authored over 100 scientific publications in the fields of radio-frequency identification (RFID) antenna design and industrial RFID applications. Her research interests are focused on RFID antenna development for tags, readers, and RFID sensors.

**Toni Björninen** (M'08) received the M.Sc. degree in electrical engineering in 2009 from Tampere University of Technology (TUT), Tampere, Finland, where he is currently working toward the Ph.D. degree in electrical engineering.

He is currently a Researcher with the Department of Electronics, Rauma Research Unit, TUT. He has authored publications on passive radio-frequency identification (RFID) tag antennas and printable electronics for microwave applications. His research interests include antenna technologies for RFID systems and modeling of electromagnetics.

**Atef Z. Elsherbeni** (F'07) is a Professor of electrical engineering, the Associate Dean of Engineering for Research and Graduate Programs, the Director of the Computer-Aided Design Laboratory, School of Engineering, and the Associate Director of the Center for Applied Electromagnetic Systems Research, University of Mississippi. In 2004, he was appointed as an Adjunct Professor with the Department of Electrical Engineering and Computer Science, L.C. Smith College of Engineering and Computer Science, Syracuse University, Syracuse, NY. He has conducted research dealing with scattering and diffraction by dielectric and metal objects finite-difference time-domain analysis of passive and active microwave devices, including planar transmission lines, field visualization, and software development for electromagnetic (EM) education, interactions of EM waves with human body, radio-frequency identification and sensors development for monitoring soil moisture, airports noise levels, air quality including haze and humidity, reflector and printed antennas and antenna arrays for radars, unmanned aerial vehicles, and personal communication systems, antennas for wideband applications, antenna and material properties measurements, and hardware and software acceleration of computational techniques for electromagentics. He is the coauthor of the books "*The Finite Difference Time Domain Method for Electromagnetics With MATLAB Simulations*" (SciTech, 2009), "*Antenna Design and Visualization Using Matlab*" (SciTech, 2006), "*MATLAB Simulations for Radar Systems Design*" (CRC Press, 2003), "*Electromagnetic Scattering Using the Iterative Multiregion Technique*" (Morgan and Claypool, 2007), and "*Electromagnetics and Antenna Optimization using Taguchi's Method*" (Morgan and Claypool, 2007) and the main author of the chapters "*Handheld Antennas"* and "*The Finite Difference Time Domain Technique for Microstrip Antennas"* in the Handbook of Antennas in Wireless Communications (CRC Press, 2001).

Dr. Elsherbeni is a Fellow Member of The Applied Computational Electromagnetic Society (ACES). He is the Editor-in-Chief of the *ACES Journal* and an Associate Editor of the *Radio Science Journal*. In 2009, he was selected as Finland Distinguished Professor by the Academy of Finland, Helsinki, Finland, and Tekes.

**Lauri Sydänheimo** (M'97) received the M.Sc. and Ph.D. degrees in electrical engineering from Tampere University of Technology (TUT), Tampere, Finland.

He is currently a Professor and the Head of the Department of Electronics, TUT, and works as the Research Director of TUT's Rauma Research Unit. He has authored over 150 publications in the field of RFID tag and reader antenna design and RFID system performance improvement. His research interests are focused on wireless data communication and radio-frequency identification (RFID), particularly RFID antennas and sensors.